Available online at www.sciencedirect.com

SciVerse ScienceDirect

Journal of the European Ceramic Society 32 (2012) 727–736

www.elsevier.com/locate/jeurceramsoc

Improvements on corrosion behaviours of MgO–spinel composite refractories by addition of $ZrSiO_4$

Rasim Ceylantekin [1], Cemail Aksel *

Department of Materials Science and Engineering, Anadolu University, Iki Eylul Campus, Eskisehir 26470, Turkey

Received 2 July 2011; received in revised form 21 September 2011; accepted 1 October 2011
Available online 8 November 2011

Abstract

Corrosion behaviours of MgO–spinel–$ZrSiO_4$ compositions were investigated. The influence of corrosion resistance based on the microstructural changes occurred due to the solubilities of constituents in corroded regions was examined using SEM/EDX analysis. The following observations were determined by microstructural characterisation performed at the interface of clinker–refractory: (i) the formation of ZrO_2 and Mg_2SiO_4 phases among MgO grains after sintering, (ii) the formation of $CaZrO_3$ phase during penetration, (iii) prevention of penetration by new phases formed making a barrier effect against clinker with an improvement in densification, and (iv) the decrease in the amount of CaO and the increase in the quantity of MgO using EDX analysis made moving from clinker towards refractory. The addition of $ZrSiO_4$ reduced the values of penetration and spreading areas of the corroded regions of composite refractories and improved the corrosion resistance significantly, leading to a long service life of MgO–spinel–zircon based refractories for industrial applications.

Keywords: MgO; $MgAl_2O_4$; Zircon; Composite; Refractory; Corrosion

1. Introduction

MgO–spinel (M–S) refractories are preferred due to their displaying high thermal shock resistance in areas requiring adequate strength at high temperatures and furthermore their high corrosion resistance against basic slag, alkali attacks and molten metal abrasions.[1,2] MgO based spinel bricks are used in the cooling zone and in the upper side of the sintering zone of cement rotary kilns.[3,4] In cement rotary kilns, alkali compounds coming from raw materials and fuel evaporate depending on temperature when they reach the upper transition zone of the kiln.[5,6] Alkali compounds in vapour form infiltrate through the pores of bricks and make progress towards cold regions in the body of the brick. With also the aid of calcium silicates, they react not only among each other but also with brick components and settle in the pores of the bricks. The created alkali compounds condense while they continue to propagate in the body of the brick and crystallize when they find appropriate temperatures. For example; when clinker having low viscosity goes into reaction with spinel, it forms Montisellite ($CaO.MgO.SiO_2$) that is a compound with relatively lower melting points (1360 and 1490 °C).[7] For this reason, the bonding structure of the brick is either destructed or detached and accordingly corrosion resistance, structural stability, thermal shock performance and elastic properties may change. It is therefore necessary to preserve the minimum ratio and to determine the optimum particle size distribution in the contents of spinel.[8] MgO–spinel refractories containing a small amount of spinel display high resistance against thermo-mechanical stresses formed at high temperatures and resultant thermal shocks. Addition of relatively high amounts of spinel leads to an increase in resistance against chemical attacks and corrosion; however, this decreases the resistance of MgO–spinel refractories against thermal shocks.[9] Therefore, high resistance against both corrosion including alkali attacks and thermal shocks in MgO–spinel bricks must be achieved through optimization of the amount of added spinel for these two aspects.

Corrosion can be considered as the debonding and subsequent physical fragmentation of the refractory, due to destruction of the bonds via the liquid phase occasioned by molten slag or clinker,

* Corresponding author. Tel.: +90 222 3350580x6362; fax: +90 222 3239501.
E-mail address: caksel@anadolu.edu.tr (C. Aksel).
[1] Present address: Department of Ceramic Engineering, Dumlupınar University, Merkez Campus, Kutahya 43100, Turkey.

0955-2219/$ – see front matter © 2011 Elsevier Ltd. All rights reserved.
doi:10.1016/j.jeurceramsoc.2011.10.005

together with the chemical dissolution of all phases.[10,11] The damage caused on large grains by means of the liquid phase formed by molten slag or clinker is at a lower level than the damage on small grains due to their smaller surface areas.[12] Factors determining the reactivity and solubility of the matrix phase are the amount of accessible porosity in the refractory exposed to corrosion through penetration of molten slag and the wetting/spreading capability of the liquid phase formed by molten glass/clinker on the surface of the refractory.[13,14] It is reported that the incorporations of additives into MgO–spinel improve the densification behaviour of those composite refractories.[15,16] However, the effect of constituents that may be added to MgO–spinel refractories on corrosion behaviour is not discussed in detail in sources. Therefore, it has become necessary to support and investigate the basic factors affecting corrosion resistance through additional studies. Enhancement of corrosion resistance through addition of zircon into M–S refractories used at high temperatures during service in the industry is the basis for this research. In this study, significant improvements have been achieved in the corrosion resistance of new composite refractory materials obtained by determination of optimum compositions as a result of addition of zircon in varying proportions into MgO–spinel refractories and the parameters/mechanisms affecting such factors have been investigated in detail with their causes.

2. Experimental

Various recipes were prepared by adding 5, 10, 20 and 30 wt.% zircon ($ZrSiO_4$) to compositions obtained from incorporations of 5%, 10%, 20% and 30% $MgAl_2O_4$ spinel (S) by weight into MgO (M). Batches were prepared using MgO (0–1 mm), spinel (0–1 mm) and zircon (~13 μm). Materials produced for determining the interaction of M–S and M–S–zircon containing composite refractories with cement clinker were prepared in two different shapes as (i) in cylinder form (diameter ~50 mm, height: ~50 mm) by drilling a hole on top (diameter ~18 mm, depth: ~20 mm) and (ii) in the square shaped ($10 \times 10\,cm^2$) samples. On samples shaped from batches prepared for the production of cylindrical and square shaped refractories, there was a difference in press pressures as a result of their having different surface areas though similar forces were applied to different types of these materials. The press pressures applied for cylindrical and square shaped specimens were therefore ~175 MPa and ~35 MPa, respectively. The sintering temperature of all samples was ~1600 °C and dwelling time at maximum temperature was about ≥10 h. After three samples were cut from each material having different compositions, they were boiled for two hours in water. Bulk density and apparent porosity values were then measured by the standard method[17] and average values were taken. The bulk density (ρ) and apparent porosity values of cylindrical and square samples were measured for both due to the difference in press pressures applied. X-ray diffraction (XRD) measurements were carried out using Rigaku RINT2000 equipment. Scanning electron microscope (SEM) studies were carried out using Zeis Evo 50 device with the microstructures of materials analyzed. Using photographs taken on the surfaces of specimens, which were polished and thermally etched for 10 min at 1450 °C, the average MgO grain size was calculated using a standard line mean intercept method.[18]

Corrosion tests were performed under the standard conditions in two different ways for cylindrical and square samples.[19,20] In the first one, 8 g cement clinker passing through 63 μm sieve was added to samples prepared in cylindrical shape by drilling a hole on top. Then, corrosion tests were performed statically using 10 °C/min of heating and cooling rates where the dwelling time was 72 h at 1500 °C in the kiln (Nabertherm HT16/18). To examine the cross-section of specimens where clinker has penetrated the refractory, samples were cut by a diamond disc 1.5 mm thick into half and their surfaces were cleaned for ~2 min using respectively 320, 800 and 1200 grade SiC papers and subsequently polished. For each sample having a different composition, the dimensions of the corroded region (e.g. distance of penetration occurring on clinker–refractory interface or length of region where clinker penetrates the refractory) were measured minimum ≥3 times at various regions with 'Digital Measurement Microscope' (MAHR GmbH, Model: WMS). The average values of those measurements were then determined with precision. Subsequently, microstructural changes that may occur in the regions at the interface of clinker–refractory were examined in detail with SEM in the region where refractory material was corroded: (i) initial section where clinker starts to penetrate into refractory (Region I close to clinker), (ii) medium region remaining between clinker and refractory (Region II) and (iii) end section where penetration of clinker into refractory terminates (Region III close to refractory). In addition, the solubility of different constituents at the interface of clinker–refractory was evaluated by EDX analyses of different zones. The effect of microstructural changes that might occur as a result of solubility of constituents at the interface of clinker–refractory on corrosion resistance was investigated.

In the second type of corrosion tests applied on samples prepared in square shape, 4 g cement clinker passing through 63 μm sieve was placed by means of a 22 mm-diameter mould to be lined up with the centre of the square on the surface of each refractory having different compositions for fixing the initial surface area in order to determine the spreading amount of cement clinker on refractories. Subsequently, static corrosion tests were performed using 10 °C/min of heating and cooling rates where the dwelling time was 72 h at 1500 °C. Photographs of spreading areas of cement clinker on the surface of refractory materials were taken and measurements were done using Image J program (http://www.ansci.wisc.edu/equine/parrish/index.html) and a digital callipers. For calculation of the spreading areas of each sample having a different composition, ~50 diameters were measured from different directions on the trace left by the cement clinker on the square sample and their average values were used. The spreading/wetting areas formed by cement clinker on the surface of refractory materials were determined and their influence on corrosion resistance was examined. Optimum compositions displaying high corrosion resistance were determined in M–S–zircon containing refractories obtained

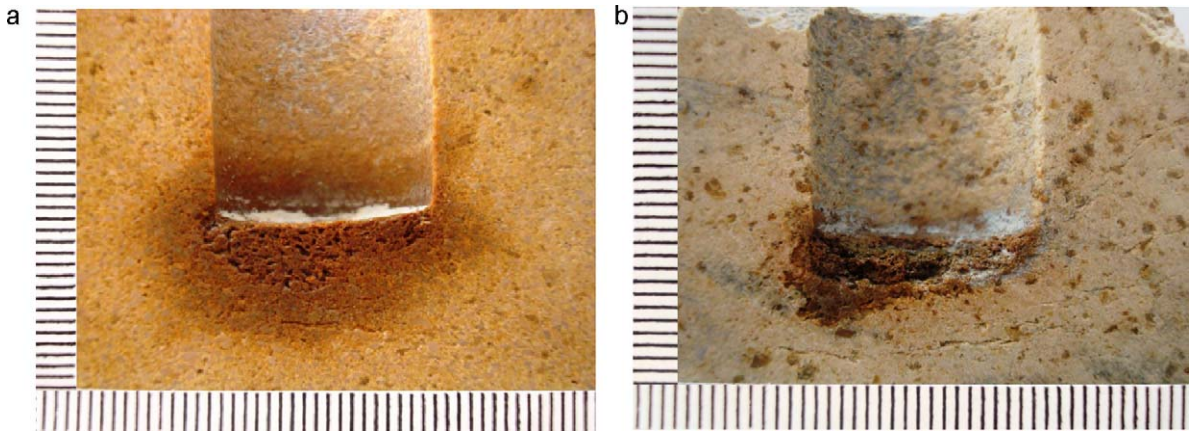

Fig. 1. Refractory materials containing (a) M–30%S and (b) M–30%S–30%zircon that were prepared in cylindrical form and corrosion tested (scale: 1 mm).

from incorporation of various amounts of $ZrSiO_4$ into M–S refractories containing spinel in varying percentages.

3. Results and discussion

Zircon ($ZrSiO_4$) was introduced in the amounts of 5%, 10%, 20% and 30% into MgO–Spinel (M–S) composite refractories containing 5%, 10%, 20% and 30% $MgAl_2O_4$ spinel (S). The results of corrosion tests performed by placing clinker into $20 \times 18\,mm^2$ holes opened on composite refractories produced as cylinders in $50 \times 50\,mm^2$ length and diameter are given below. Additives as used in figures and the table denote: (i) $MgAl_2O_4$ for M–S refractories and (ii) $ZrSiO_4$ for M–S–zircon materials.

Model samples are given in Fig. 1. The examination of regions corroded due to the penetration of cement clinker into refractory materials has shown that the amount of penetration decreased with the addition of zircon into M–S (Fig. 1). Relative density and apparent porosity results are given in Figs. 2 and 3, respectively. The relative density values of M–S–zircon containing samples prepared by addition of zircon continuously improved with the increasing amount of zircon as compared to M–S materials. There was a significant increase in bulk density values leading to an enhancement of relative density with the addition of an additive with greater density (ρ_{Zircon}: $4.56\,g/cm^3$)[21,22] to M–S compositions (ρ_{M-S}: $3.58\,g/cm^3$)[21,22] (Fig. 2). During sintering for zircon added refractories, when MgO forming the main phase reacts with SiO_2 released after decomposition of zircon as (i) SiO_2 and (ii) ZrO_2, a stronger bond is created between the additive and the grains of main constituent due to the formation of forsterite (Mg_2SiO_4) phase and thus sintering becomes more effective.[23] On the other hand, the apparent porosity values of M–S–zircon containing refractories are lower than those of M–S materials and decrease as the amount of zircon increases (Fig. 3). It was observed that the effect of using zircon on apparent porosity is higher than that of spinel.

The change in the values of penetration distance in regions where clinker causes corrosion (Fig. 1) as a function of amount of additives in materials produced with the introduction of spinel to MgO and $ZrSiO_4$ to M–S compositions is given in Fig. 4. The penetration distance of cement clinker in the refractory prepared using M–S–zircon components is lower than that of M–S refractories except for M–S–5%zircon and decreases as the amount of zircon increases (Fig. 4). Penetration of clinker into refractory material has taken place at a minimum level in M–30%S–30%zircon composition with an improvement of 2.2-fold as an example compared to M–30%S. It was observed that

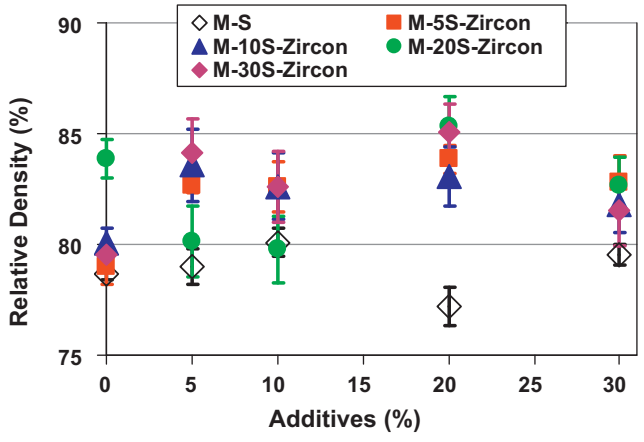

Fig. 2. Relative density as a function of additives.

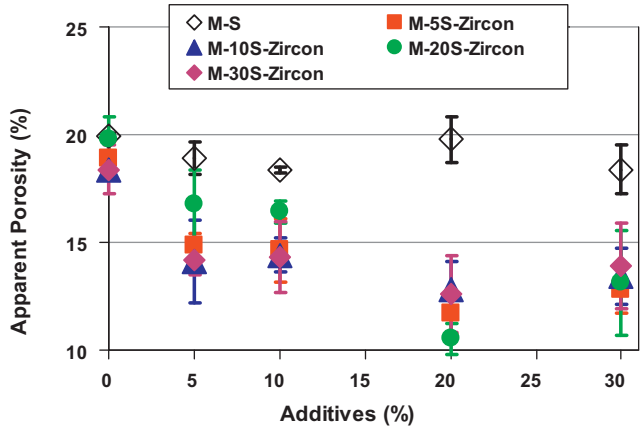

Fig. 3. Apparent porosity as a function of additives.

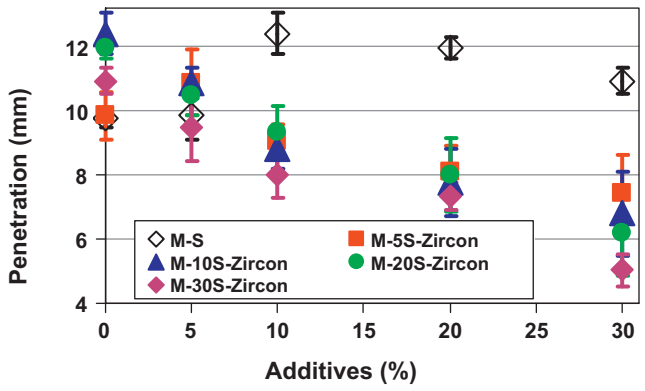

Fig. 4. Penetration distance values as a function of additives.

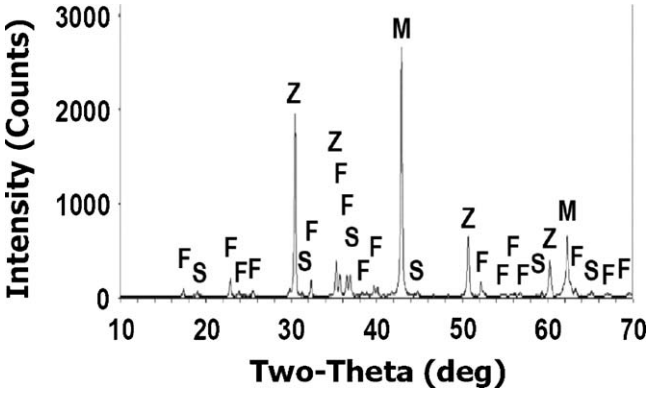

Fig. 6. XRD graph of a composite refractory having M–20%S–20%zircon composition where measurement was performed before corrosion test (M: MgO, S: $MgAl_2O_4$, Z: ZrO_2 and F: Mg_2SiO_4).

the addition of zircon into M–S materials increases corrosion resistance significantly.

For the compositions where spinel was added to MgO and zircon was incorporated into M–S, the change in the values of penetration distance at the clinker–refractory interface as a function of apparent porosity is given in Fig. 5. M–S–zircon refractories have a much lower quantity of pores and a much wider pore scattering compared to M–S materials. In a few of the M–S–zircon compositions, although the amount of apparent porosity had increased very little, there was a slight reduction observed in the measured penetration values. This may arise from the regions corroded at the interface of clinker–refractory after corrosion tests limiting measuring precision due to lack of homogeneity in certain samples and thus a relatively wide scattering of standard deviations. When M–S and M–S–zircon refractories were compared, it was generally observed that introduction of zircon caused a significant decrease in the amount of apparent porosity and therefore a marked reduction in the amount of penetration. For this reason, the amount of apparent porosity has been determined as one of the important parameters affecting the corrosion resistance of M–S–zircon containing refractories. In addition to these, although the apparent porosity values of M–S–30%zircon refractories is relatively higher than those of M–S–20%zircon, the composition where the penetration distance of refractories at a minimum is M–S–30%zircon.

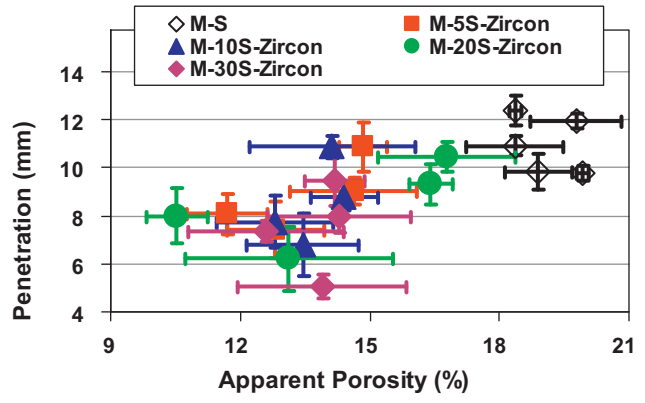

Fig. 5. Penetration distance values as a function of apparent porosity.

This indicates that zircon content is also important together with the amount of porosity (Figs. 3–5).

X-ray diffraction (XRD) measurements of M–S–zircon compositions were performed before and after corrosion tests on cylindrical shaped samples. The results of XRD before corrosion testing for the sintered sample with a composition of M–20%S–20%zircon having maximum relative density (i.e. bulk density) are given in Fig. 6. According to the phase analysis results; forsterite (Mg_2SiO_4) and cubic zirconia phases were identified besides MgO and spinel phases. A stronger bond is formed between the additive and the grains of main constituent due to the formation of forsterite phase as a consequence of the reaction between SiO_2, which is released after dissociation of zircon as ZrO_2 and SiO_2 during sintering, and MgO that is the main phase. It was determined that sintering was more effective with the formation of new phases. This was consistent with the increase in relative density values and accordingly the decrease in the amount of apparent porosity, as the quantity of zircon added to M–S materials increased. In addition; after performing corrosion tests, XRD analysis of corroded region at the interface of cement clinker and refractory having M–20%S–20%zircon composition displaying the lowest apparent porosity data was carried out. Fig. 7 shows that $CaZrO_3$ phase was formed during penetration when CaO present in the clinker reacted with ZrO_2, which was released due to the decomposition of zircon, as well as the identification of MgO, spinel and zirconia phases.

Images of various corrosion regions taken by scanning electron microscope (SEM) of composite refractories for which corrosion test was performed, produced by adding 30% zircon to MgO–30%Spinel as cylinders of 50 × 50 mm^2 length and diameter are given in Fig. 8. The results of EDX analysis (Table 1) and the mappings including both microstructural images of the different corroded regions at the clinker–refractory interface and the distributions of present elements (Figs. 9 and 10) are analyzed. The areas close to clinker (Region I), located in the middle of clinker and refractory (Region II) and close to the refractory (Region III) were examined.

In general, zirconia particles released following dissociation of zircon are concentrated in the perimeter of regions containing clinker and are distributed both at grain boundaries and

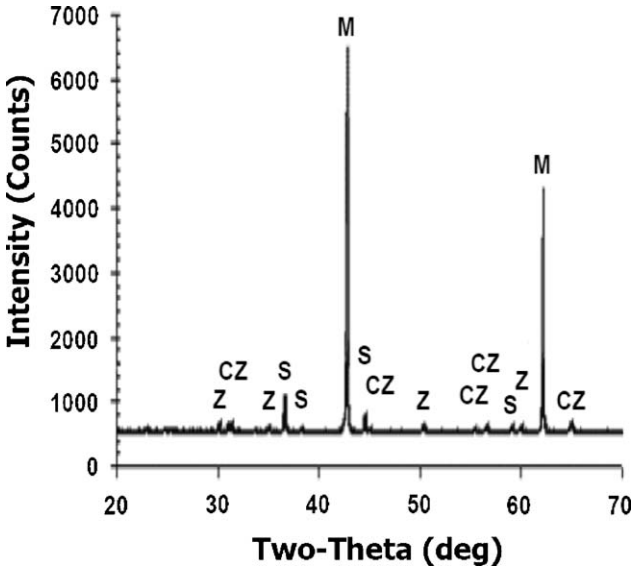

Fig. 7. XRD graph of a composite refractory having M–20%S–20%zircon composition where measurement was performed after corrosion test (M: MgO, S: $MgAl_2O_4$, Z: ZrO_2 and CZ: $CaZrO_3$).

within the MgO grains (Figs. 8–10). The microstructure of M–30%S–30%zircon composition changes moving from the region in which penetration starts to the refractory region where infiltration decreases (Figs. 8–10). Refractory material was corroded effectively in areas where no white coloured ZrO_2 grains were found in the region close to clinker (Figs. 8a and 9). However, moving towards the refractory region with less penetration, corroded areas decrease with the increase in the concentration of ZrO_2 particles (Figs. 8b, 8c and 10). When the microstructures and distribution of elements of M–30%S–30%zircon refractories were analyzed, it was observed that penetration of cement clinker into MgO grains present in the refractory body is more distinct in regions at the beginning stage of infiltration. It was also determined that the penetration into MgO grains decreases significantly towards the refractory at the clinker–refractory interface in the corroded region (Figs. 8–10). Similarly, while the amount of MgO increased in the results of the EDX analysis done on areas from the beginning of penetration (Region I) to the end of penetration (Regions II and III); the amount of CaO decreased (Table 1). For different regions, determination of concentrations of CaO that is one of the most important basic constituents of cement clinker is one of the basic parameters assisting in determination of the corrosion level of the refractory material. EDX analysis shows that the amount of CaO is high in the section where penetration starts (Region I). Furthermore, it is systematically decreasing in a periodic manner towards the middle region (Region II) and the third region (Region III) that is close to the refractory. It was therefore confirmed by EDX and microstructural analysis that the penetration observed in the microstructure from the beginning to the end of the corroded region decreases (Table 1; Figs. 8–10).

An examination of the distribution of elements under microstructural analyses shows that in general (i) MgO and SiO_2 and (ii) CaO and ZrO_2 distributions are located in similar regions (Figs. 9 and 10). A stronger bonding takes place

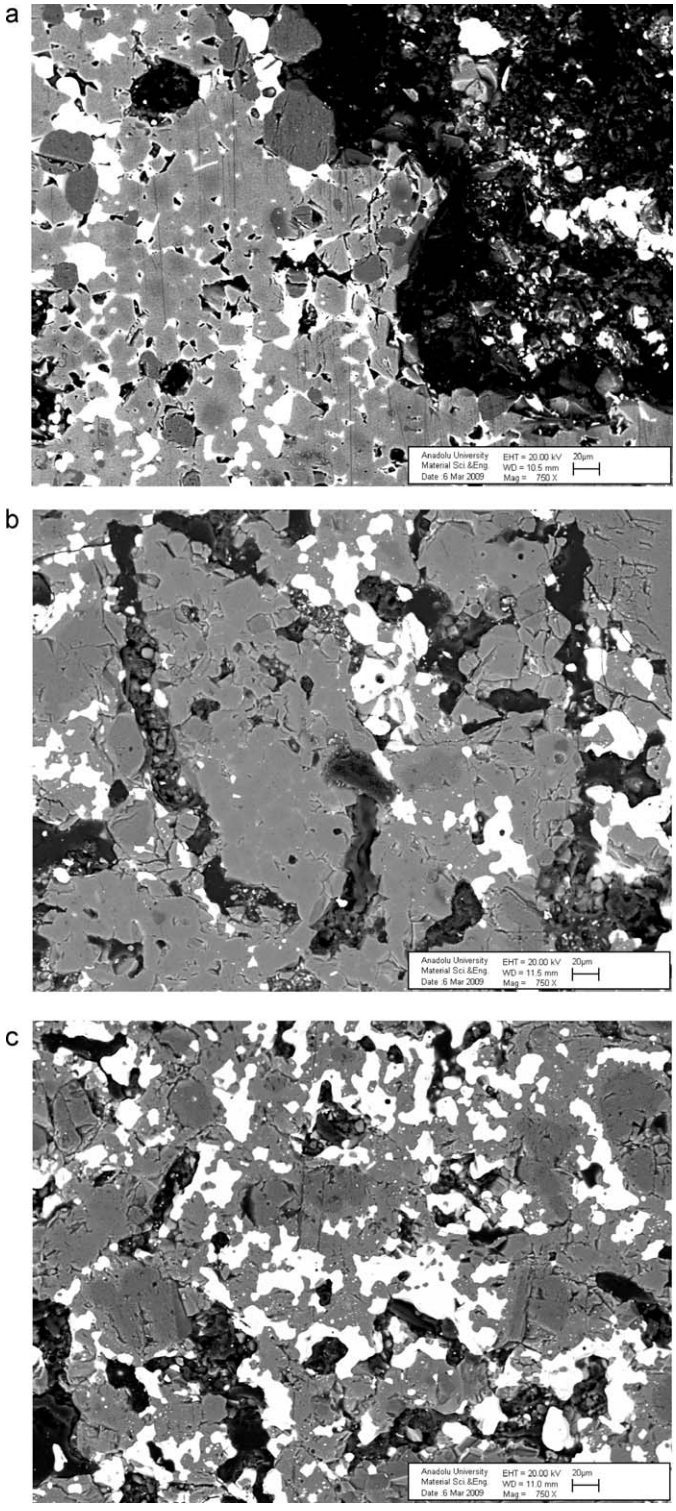

Fig. 8. Microstructural images in different regions of corroded material having M–30%S–30%zircon composition (scale bar: 20 μm): (a) Region I close to clinker, (b) middle Region II and (c) Region III close to refractory.

between the additive and the grains of main constituent due to formation of forsterite (Mg_2SiO_4) phase as a result of the reaction between MgO and SiO_2, which is released following the decomposition of zircon as ZrO_2 and SiO_2, during sintering (Figs. 6, 9 and 10). Furthermore, it is observed that $CaZrO_3$

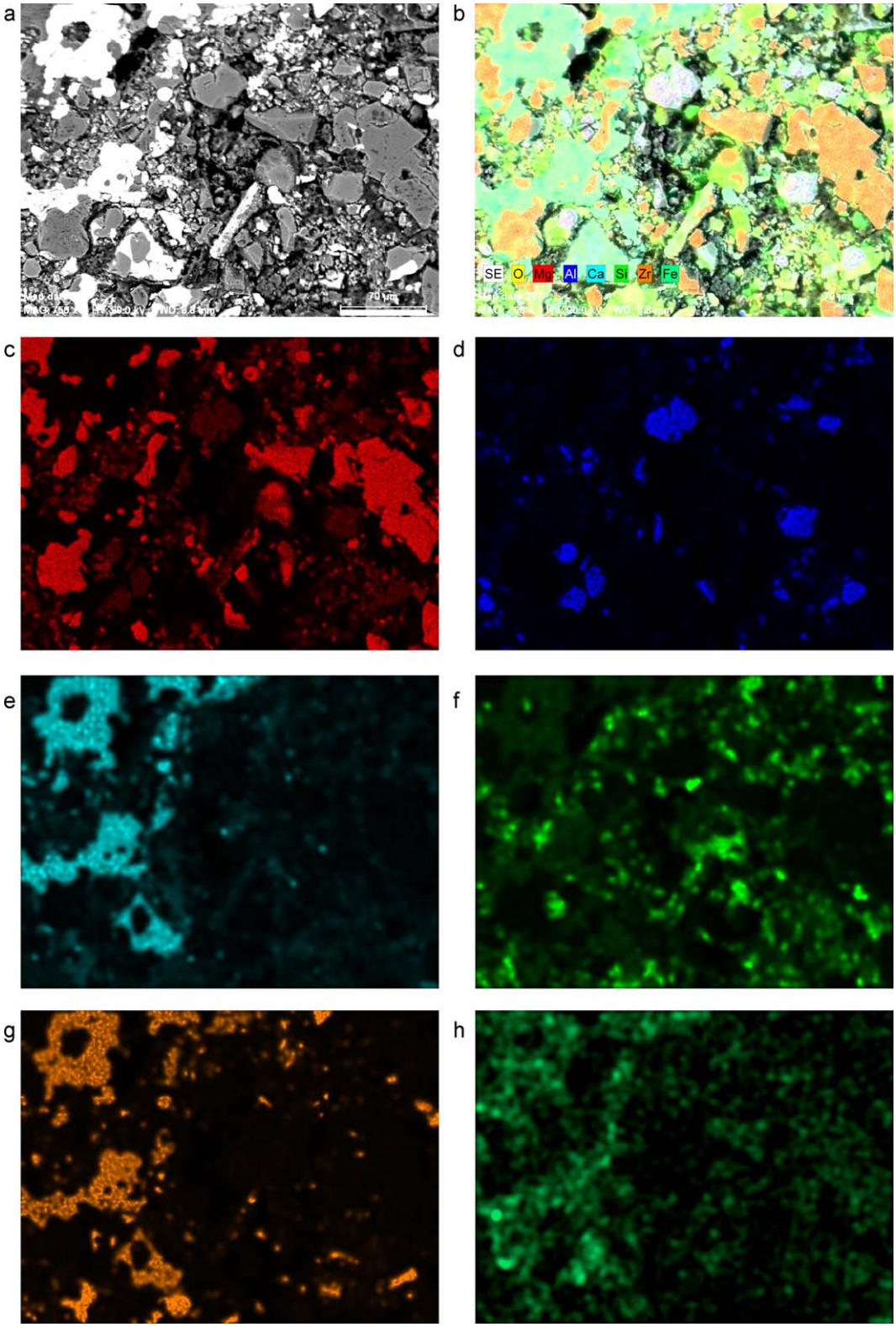

Fig. 9. Microstructural image of corroded Region I (scale bar: 70 μm): close to clinker at the interface of cement clinker and refractory having M–30%S–30%zircon composition [(a) and (b)], and distribution of elements [(c) Mg, (d) Al, (e) Ca, (f) Si, (g) Zr and (h) Fe].

phase also formed during penetration when CaO present in the clinker reacted with ZrO_2 released due to the dissociation of zircon (Figs. 7, 9 and 10). The formation of these new phases was confirmed by XRD analysis (Figs. 6 and 7). In addition, although the Ca^{2+} and Si^{4+} elements were distributed in the quite different zones in the region close to clinker (Fig. 9), the distributions of these elements were located in the similar areas towards the region close to the refractory (Fig. 10). However,

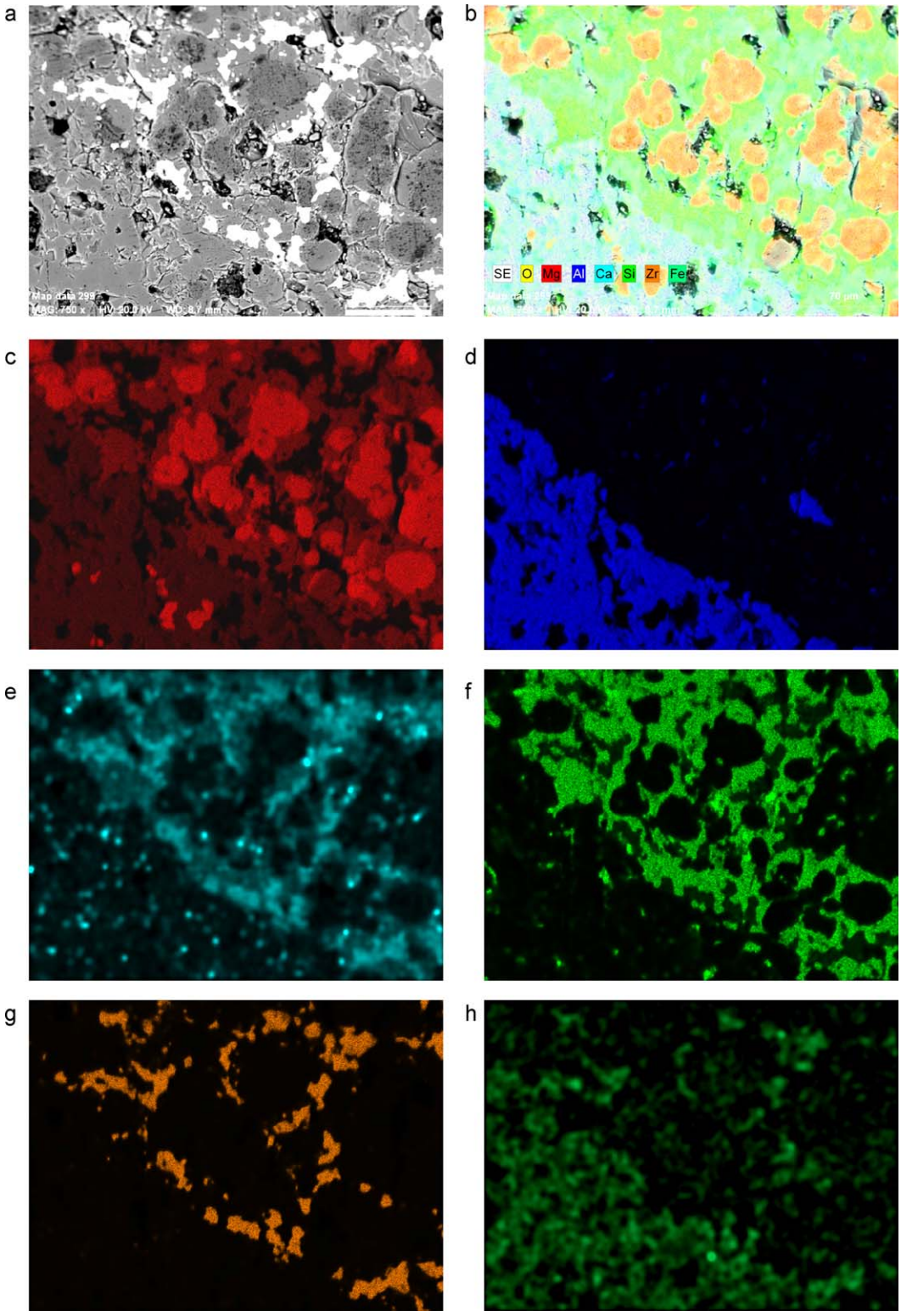

Fig. 10. Microstructural image of corroded Region III (scale bar: 70 μm): close to refractory at the interface of cement clinker and refractory having M–30%S–30%zircon composition [(a) and (b)], and distribution of elements [(c) Mg, (d) Al, (e) Ca, (f) Si, (g) Zr and (h) Fe].

XRD results confirmed that there was not any reaction between CaO and SiO_2 leading to formation of new calcium–silicate phases in the corroded region during penetration (Fig. 7). It clarifies that the variation in the SiO_2 distribution basically depends on the location of MgO grains. After the reaction between MgO and SiO_2 leading to formation of forsterite phase during sintering (Fig. 6), SiO_2 that had already reacted with MgO did not react with CaO again at the clinker–refractory interface during penetration (Fig. 7). Fig. 10 shows that both (i) Mg_2SiO_4 and (ii) $CaZrO_3$ phases formed that were located in areas in close

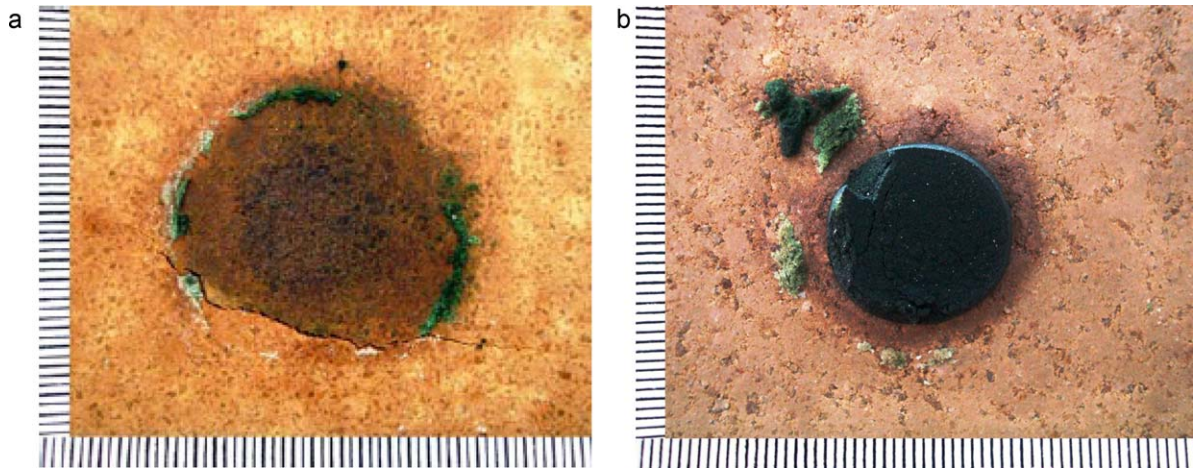

Fig. 11. Refractory materials containing (a) M–30%S and (b) M–30%S–30%zircon prepared in square form and corrosion tested (scale: 1 mm).

proximity to each other where (i) Mg^{2+} and Si^{4+} forming Mg_2SiO_4 and (ii) Ca^{2+} and Zr^{4+} elements forming $CaZrO_3$ were also separately overlapping in the areas towards the region close to the refractory. It is observed that they were both effective phases (i.e. Mg_2SiO_4 and $CaZrO_3$) in preventing the penetration of clinker into the refractory that lead to an improvement in corrosion resistance. It is also determined that the formation of $CaZrO_3$ phase in the region close to clinker is limited and it covers smaller regions in the microstructure, which indicates a high amount of infiltration (Fig. 9). However, there is a more homogeneous distribution of $CaZrO_3$ phases occupying relatively greater amount of areas with a much wider scattering in the region close to refractory that exhibits a lesser amount of penetration (Fig. 10). It is detected that clinker did not infiltrate into the regions where (i) phases forming after sintering (i.e. ZrO_2 and forsterite) and (ii) $CaZrO_3$ phase forming during penetration in the corroded area in the refractory were present and stopped when it reached to these regions (Figs. 8–10). In general, densification has increased with the addition of zircon and infiltration/penetration of clinker into the refractory material becomes harder as newly formed phases act as barriers and hence corrosion resistance is enhanced.

In addition to measurements of penetration distances in regions where clinker led to corrosion in M–S and M–S–zircon containing refractories having different compositions, corrosion tests were also performed on $10 \times 10\,cm^2$ square samples. Then, the spreading areas of clinker were determined. Exemplar samples from M–S and M–S–zircon compositions are given in Fig. 11.

The amount of the spreading of cement clinker on composite refractory materials prepared with M–S–zircon components has risen when 5% zircon is added to all M–S compositions containing spinel in varying percentages. However, it drops sharply when 10% zircon is incorporated into each M–S material. Then, the spreading area is decreasing relatively at a smaller slope when higher percentages of zircon is used (Fig. 12). In the M–30%S–zircon compositions, as the amount of zircon was increased, the spreading area values have dropped significantly. For example, when M–30%S–30%zircon materials exposed to minimum penetration was compared with M–30%S composition, spreading area has decreased by 43% with a 1.8-fold improvement observed in terms of corrosion resistance (Fig. 12).

The relative density and apparent porosity results of square and cylindrical shaped samples showed a similar trend to each other. For square samples, relative density values increased and accordingly apparent porosity data decreased periodically with increasing amount of zircon added in M–S compositions. The changes of the spreading area values formed by clinker on the surface of refractory in M–S and M–S–zircon compositions as a function of the amount of apparent porosity are given in Fig. 13. In general, it was observed that as the quantity of apparent porosity decreased, the spreading area values of clinker also decreased. The significant decrease in the amount of apparent porosity with the introduction of zircon has led to a decrease in the corrosion level and it was verified that the quantity of pores is an important parameter affecting corrosion resistance.

In addition, average MgO grain size of sintered samples before corrosion testing was calculated for different compositions as: (i) pure MgO = 67 μm, (ii) M–5%S = 40 μm and (iii) M–5%S–20%$ZrSiO_4$ = 27.5 μm being reduced significantly with the increase in the amount of additives. It is well known that

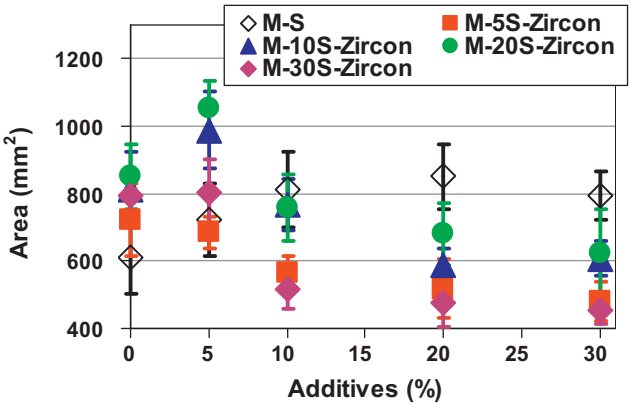

Fig. 12. Spreading area values as a function of additives.

Table 1
EDX analyses of (i) clinker, (ii) Region I close to clinker, (iii) Region II in the middle of clinker–refractory and (iv) Region III close to refractory in the corroded area on a refractory material containing M–30%S–30%zircon constituents.

M–30%S–30%zircon: chemical composition (%)								
Regions	MgO	CaO	Al_2O_3	SiO_2	ZrO_2	Fe_2O_3	K_2O	Total
Clinker	1.28	70.64	3.97	18.73	–	3.12	2.26	100.00
I	43.64	4.70	23.34	2.81	22.41	3.10	–	100.00
II	43.82	1.97	12.08	15.14	25.89	1.10	–	100.00
III	55.72	0.85	18.22	8.46	15.26	1.49	–	100.00

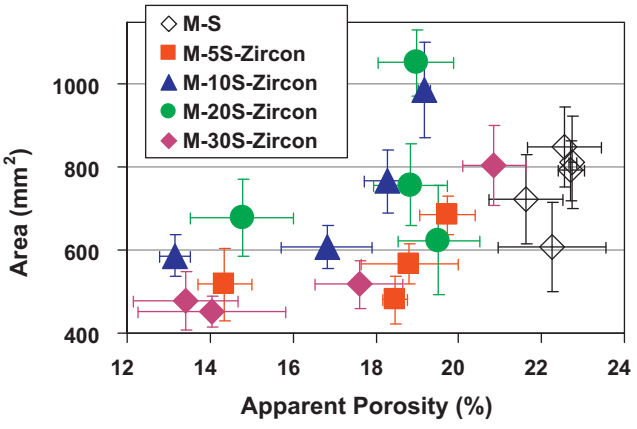

Fig. 13. Spreading area values as a function of apparent porosity.

the damage caused on large grains via the liquid phase formed by molten slag or clinker is at a lower level than the damage on small grains due to their smaller surface areas.[12] It was stated that a marked reduction in mean MgO grain size occurred by the incorporation of additives into MgO was therefore not related with the improvement on corrosion resistance of M–S–zircon containing composite refractory materials.

In general, it was observed that in great majority of M–S and M–S–zircon containing compositions, the distance of penetration and the spreading area values occasioned by clinker on refractory materials are consistent with each other (Figs. 4 and 12). Penetration resistance of spinel added M–S materials is at a limited level compared to M–S–zircon compositions (Fig. 1). Zircon addition increases the bulk density significantly by filling the pores, hence decreasing the quantity of pores and leading to the described microstructural changes. For example, in the distance of penetration and spreading area of material of M–30%S–30%zircon composition, respectively 2.2 and 1.8-fold improvements in comparison with M–30%S were achieved (Figs. 1, 4, 11 and 12). This increase observed in the corrosion resistance is consistent with M–S–zircon containing refractory materials having a longer useful life in service.

4. Conclusions

The distance of penetration and spreading area values occasioned by cement clinker on M–S–zircon refractories decreased significantly as the quantity of introduced zircon was increased and the results were consistent with each other. The clinker infiltration was at a limited level in regions where (i) post-sintering phases (ZrO_2 and Mg_2SiO_4) and (ii) $CaZrO_3$ phases that form during penetration in the corroded region of refractory materials were present. As a result of the formed new phases serving as a barrier, penetration of clinker into the refractory becomes difficult and therefore this leads to an increase in corrosion resistance. While moving from the corroded region towards the refractory at the interface of clinker–refractory, the penetration into MgO grains decreased significantly due to the marked drop in the CaO quantity. With the incorporation of zircon, the formation of these stated microstructural changes and the development in densification leading to decrease in the amount of apparent porosity have been identified as significant parameters affecting the corrosion resistance of M–S–zircon containing refractories. Improvements have been achieved at the penetration distance and spreading area of a material having M–30%S–30%zircon composition in comparison with M–30%S by factors of 2.2 and 1.8, respectively. This improvement in corrosion resistance is also associated with a long service life of M–S–zircon based refractories for industrial applications.

Acknowledgements

This study was partly supported by Anadolu University and in part TUBITAK under project no: 106M394 with partial support provided also by Konya Selcuklu Krom Magnezit Tugla Sanayi A.S. We would like to express our gratitude to A. Ozkaymak, R. Ozbasi, O. Bezirci, and all agency employees and personnel involved in this project for their support. We also thank the agencies and plant authorities for the supplied equipments and raw materials.

References

1. Eusner GR, Hubble DH. Technology of spinel bonded periclase brick. *J Am Ceram Soc* 1960;**43**:292–6.
2. Aksel C, Riley FL. Magnesia–spinel ($MgAl_2O_4$) refractory ceramic composites. In: Low IM, editor. *Ceramic matrix composites: microstructure, properties and applications*. USA: Woodhead Publishing Limited and CRC Press LLC; 2006. p. 359–99.
3. Benbow J. Cement kiln refractories-down to basics. *Ind Miner* 1990;**268**:37–45.
4. Uchikawa H, Hagiwara H, Shirasaka M, Watanabe T. Application of periclase–spinel bricks to cement rotary kiln in Japan. *Interceram Spec Issue* 1984;**33**:386–406.
5. Harburg HKF. Experience with magnesium–aluminium–spinel bricks in a 3000 t/d rotary kiln. *Zement-Kalk-Gibs Int* 1993;**3/4**:446–54.
6. Tokunaga K, Kozuka H, Honda T, Tanemura F. Further improvements in high temperature strength, coating adherence, and corrosion resistance

of magnesia–spinel bricks for rotary cement kiln. In: *Proc UNITECR'91 Congress*. Aachen, Germany. 1991. pp. 431–435.
7. Gabis V, Graba L. Microstructure of reaction-sintered spinel/corundum refractories prepared from various alumina–magnesia mixtures. Euro Ceram II, Electroceramics and Ceramics for Special Applications. *Proc. 2nd European Ceram Soc Conf*. Augsburg, Germany, 1991, Vol. 3, pp. 2593–2598.
8. Aksel C, Riley FL. Effect of particle size distribution of spinel on the mechanical properties and thermal shock performance of MgO–spinel composites. *J Eur Ceram Soc* 2003;**23**:3079–87.
9. Moore B, Frith M, Evans D. Developments in basic refractories for cement kilns. *World Cement* 1991;**12**:5–12.
10. Aksel C, Riley FL, Konieczny F. The corrosion resistance of alumina–mullite–zircon refractories in molten glass. *Euro Ceram VIII Key Eng Mater* 2004;**264–268**:1803–6.
11. Zhang S, Lee WE. Use of phase diagrams in studies of refractories corrosion. *Int Mater Rev* 2000;**45**:41–58.
12. Lee WE, Rainforth WM. Refractories. In: *Ceramic microstructures: property control by processing*. London, UK: Chapman & Hall; 1994. p. 452–508.
13. Aksel C. The microstructural features of an alumina–mullite–zirconia refractory material corroded by molten glass. *Ceram Int* 2003;**29**: 305–9.
14. Aksel C, Dexet M, Logen N, Porte F, Riley FL, Konieczny F. The influence of zircon in a model aluminosilicate glass tank forehearth refractory. *J Eur Ceram Soc* 2003;**23**:2083–8.
15. Sarkar R, Das SK, Banerjee G. Effect of additives on the densification of reaction sintered and presynthesised spinels. *Ceram Int* 2003;**29**:55–9.
16. Sarkar R, Tripathi HS, Ghosh A. Reaction sintering of different spinel compositions in the presence of Y_2O_3. *Mater Lett* 2004;**58**: 2186–91.
17. BS 7134. Methods for determination of density and porosity. *British Standard Testing of Engineering Ceramics, Part 1, Section 1.2*; 1989.
18. Mendelson MI. Average grain size in polycrystalline ceramics. *J Am Ceram Soc* 1969;**52**:443–6.
19. McCauley RA. Corrosion test procedures. In: *Corrosion of ceramics*. New York, USA: Marcel Dekker Inc.; 1995. p. 109–27.
20. Chesters JH. Testing refractories. In: *Refractories: production and properties*. London: The Iron and Steel Institute; 1973. p. 1–65.
21. Shackelford JF, Alexander W, Park JS, editors. *CRC materials science and engineering handbook*. Boca Raton, FL: CRC Press; 1994.
22. Burnett SJ. *Properties of refractory materials*. Harwell: UKAEA Research Group Report; 1969.
23. Ceylantekin R. *The effects of $ZrSiO_4$ and ZrO_2 additions on mechanical, thermal shock and corrosion behaviours of $MgO–MgAl_2O_4$ refractories*. PhD thesis. Anadolu University, Eskisehir, Turkey; 2009.